

Multimode Q Control in Tapping-Mode AFM: Enabling Imaging on Higher Flexural Eigenmodes

Michael G. Ruppert, *Student Member, IEEE*, and S. O. Reza Moheimani, *Fellow, IEEE*

Abstract—Numerous dynamic atomic force microscopy (AFM) methods have appeared in recent years, which make use of the excitation and detection of higher order eigenmodes of the microcantilever. The ability to control these modes and their responses to excitation is believed to be the key to unraveling the true potential of these methods. In this paper, we highlight a multimode Q control method that exhibits remarkable damping performance and stability robustness. The experimental results obtained in ambient conditions demonstrate improved imaging stability by damping nondriven resonant modes when scanning is performed at a higher eigenmode of the cantilever. Higher scan speeds are shown to result from a decrease in transient response time.

Index Terms—Atomic force microscopy, controller design, optimization, positive position feedback (PPF), Q control, resonant control, vibration control.

I. INTRODUCTION

IN atomic force microscopy (AFM), a microcantilever operated in dynamic mode is a versatile and sophisticated means of interrogating samples at the nanoscale to study topographical features and inherent material properties. As the nonlinear interaction force between the tip of the cantilever and the sample surface cannot be controlled directly, conventional methods use the cantilever's response to this force to probe the surface. Responses such as the shift in cantilever resonance frequency in frequency modulation AFM (FM-AFM) [2] or the change in oscillation amplitude in tapping-mode AFM (TM-AFM) [3] have been used successfully.

In conventional TM-AFM experiments, the microcantilever is excited close to its fundamental eigenmode. Under reasonably gentle interaction forces, the resulting dynamics during imaging are well captured by modeling a single harmonic oscillator with equivalent mass, quality (Q) factor, and stiffness. However, a real cantilever has an infinite number of flexural and torsional eigenmodes. Typically, a higher

flexural eigenmode exhibits a large Q factor in ambient conditions, as well as an increased dynamic stiffness and a faster transient response and is therefore of great interest to dynamic AFM methods [4].

The benefits of using higher eigenmodes in FM-AFM are controversial. On the one hand, a small free air amplitude and increased dynamic stiffness of the higher eigenmode enable the probe to remain within the decay length of the short range interaction forces [5], [6]. It has been observed that this leads to enhanced signal-to-noise ratio due to larger frequency shifts of the higher eigenmode [7]. On the other hand, it has been reported that the Q factor of higher eigenmodes may decrease, particularly in ultrahigh vacuum, which suggests that sensitivity cannot be increased [8]–[10].

It was noted early on that if stable imaging is possible on a higher eigenmode in TM-AFM, the phase contrast due to material impurities will be significantly higher than on the fundamental eigenmode [11]. Similar results for soft samples are obtained whereas significant imaging instabilities for hard samples have been noticed [12]. These instabilities may result from the excitation of lower order eigenmodes due to the nature of the nonlinear tip-sample force. Such effects can be greatly reduced by heavily damping these nondriven lower resonant modes.

Originally introduced to modify the Q factor of the fundamental mode of the cantilever [13], Q control has led to a number of advances in TM-AFM. By actively damping the cantilever resonance, an increase in scan speed is achieved [14] while actively increasing the quality factor was shown to be beneficial to imaging sensitivity and to promoting imaging in the attractive regime [15]. The common method for active modification of the cantilever Q factor is based on differentiating or phase shifting the deflection signal to obtain velocity feedback [16]. While this time-delay method remains an easy-to-implement solution for practitioners, it comes with a number of disadvantages such as the restriction to controlling a single mode, nonrobust stability properties [16]–[18] leading to limited damping performance [19] and a nonlinear relationship between the feedback gain and desired Q factor [20]. This problem can be overcome by using integrated actuation, e.g., via a piezoelectric layer which enables the utilization of resonant controllers that guarantee robust closed-loop stability when used in a collocated sensor-actuator environment [21].

Previously, we have demonstrated how imaging on the second eigenmode with a lower Q factor leads to improved tracking performance at high scan speeds in TM-AFM for rectangular scan gratings [22]. Recently, we have also shown

Manuscript received October 20, 2014; revised April 22, 2015 and July 5, 2015; accepted August 29, 2015. Manuscript received in final form September 8, 2015. Date of publication October 6, 2015; date of current version June 9, 2016. This work was supported in part by the University of Newcastle and in part by the Australian Research Council. Recommended by Associate Editor E. Usai.

M. G. Ruppert is with the School of Electrical Engineering and Computer Science, The University of Newcastle, Callaghan, NSW 2308, Australia (e-mail: michael.ruppert@uon.edu.au).

S. O. R. Moheimani was with the School of Electrical Engineering and Computer Science, The University of Newcastle, Callaghan, NSW 2308, Australia. He is now with the Department of Mechanical Engineering, University of Texas at Dallas, Richardson, TX 75080 USA (e-mail: reza.moheimani@utdallas.edu).

Color versions of one or more of the figures in this paper are available online at <http://ieeexplore.ieee.org>.

Digital Object Identifier 10.1109/TCST.2015.2478077

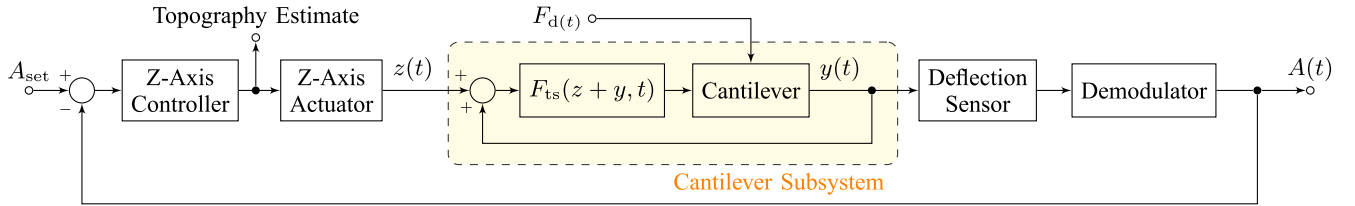


Fig. 1. Schematic setup of the AFM feedback system highlighting the main components and internal feedback nature of the cantilever in contact with a sample.

experimental results on controlling multiple Q factors in multifrequency AFM [23], which opens up new possibilities in gaining additional insights into the increased phase contrast obtained on the higher eigenmodes. In this contribution, the authors extend their previous work to the third eigenmode showing improved imaging stability and higher cantilever bandwidth while imaging nanometer features. First, we present a detailed review of the properties of higher order eigenmodes of the cantilever which, when properly used, can extend the versatility of the AFM operated in tapping-mode under ambient conditions. In contrast to the conventional time-delay method, our multimode Q control approach enables the suppression of nondriven lower order eigenmodes while at the same time offering flexible control of the driven eigenmode. The approach benefits imaging stability and renders the higher eigenmode dominant. The class of controllers used demonstrates remarkable damping performance and can be easily implemented using the standard deflection measurement of the microcantilever. Robust stability is shown to result from the collocation of actuation and sensing and intuitive robust stability results are presented which explain the high damping performance even if the negative imaginary (NI) property of the cantilever is violated. The experimental results obtained on the second and third eigenmodes verify that an increase in cantilever bandwidth can be achieved which yields better topography tracking of small features without sacrificing imaging stability.

II. HIGHER EIGENMODES OF THE MICROCANTILEVER IN ATOMIC FORCE MICROSCOPY

A. AFM Feedback System

A block diagram of the AFM operating in tapping-mode is shown in Fig. 1, highlighting the main components of the z -axis feedback loop. While the cantilever is in contact with the sample, it experiences forces due to its direct excitation F_d and due to the nonlinear tip-sample force F_{ts} . The latter is a function of the distance between the cantilever tip and the sample, i.e., the sum of the controlled z -distance between the sample and cantilever holder and the cantilever's actual feedback tip position. When the cantilever is oscillating in steady state, the output of the z -axis controller is used as a topography estimate.

B. Properties of the Higher Eigenmodes

1) *Time Constant*: For a single-mode approximation of the cantilever, the transient response exponentially decays with the time constant $\tau = 2Q/\omega_0$ [24] which is a function of

the Q factor and resonance frequency ω_0 and dictates the approximate cantilever bandwidth of

$$f_c = \frac{f_0}{2Q}. \quad (1)$$

A fast-decaying transient response is desirable since the output of the z -axis controller only resembles the surface topography when the cantilever is oscillating in steady state. Thus, when operated at a higher resonant frequency, the cantilever reacts faster to tip-sample forces, allowing the gain of the regulating z -axis controller to be increased, which yields better topography tracking.

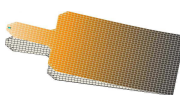
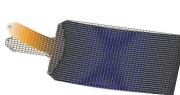
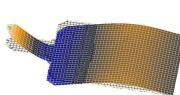
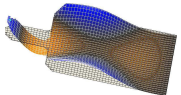
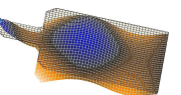
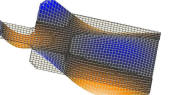
2) *Q Factor*: In contrast to findings in air where the quality factor of higher flexural eigenmodes increases [4], [25], in vacuum the Q factor of higher order modes was shown to decrease [8]–[10]. This phenomenon could be explained by the different damping mechanisms taking place. In a gaseous environment, viscous damping plays an important contribution and is shown to decrease with increasing mode number [26] due to the faster and smaller cantilever oscillations. However, in vacuum viscous damping reduces to zero and internal friction dominates the damping, which increases for higher eigenmodes due to higher stress in the structure [9]. From (1), it can be seen that the cantilever bandwidth while imaging with higher resonance frequencies is additionally increased by lowering the Q factor.

3) *Dynamic Cantilever Stiffness*: Quantitative AFM measurements require the knowledge of the spring constant of the cantilever. In quasi static AFM modes, such as force spectroscopy, the static spring constant k_c needs to be determined. The fact that the static spring constant is dominated by the spring constant of the fundamental eigenmode of the cantilever has resulted in the two being rarely distinguished from each other for dynamic AFM experiments involving the fundamental eigenmode only [27], [28]. However, when using higher eigenmodes, the dynamic spring constant k_n of the active eigenmode, which was shown to increase drastically with the mode number, needs to be determined [28].

Between the two most popular methods for calibrating cantilever spring constants, namely Sader's method [29] and the thermal noise method [30] (and its improved version in [31]), only the latter was found to be suitable for the characterization of higher eigenmode spring constants since this method does not require the knowledge of higher eigenmode shapes which are strongly affected by mass inhomogeneities such as the tip mass [28].

4) *Thermal Noise*: The theoretical vertical resolution in AFM is most prominently limited by thermal noise in the

TABLE I
 Q FACTORS (Q_i), MAGNITUDE AT RESONANCE (M_i IN DECIBELS), AND MODESHAPES OF THE FIRST SIX FLEXURAL EIGENMODES OF THE PIEZOELECTRIC CANTILEVER MEASURED BY THE AFM OPTICAL LEVER SENSOR AND WITH AN MSA-400 AT THE CANTILEVER END (MSA E), MIDDLE (MSA M), AND BASE (MSA B) AS INDICATED IN FIG. 2

	Mode 1		Mode 2		Mode 3		Mode 4		Mode 5		Mode 6	
												
	M_1	Q_1	M_2	Q_2	M_3	Q_3	M_4	Q_4	M_5	Q_5	M_6	Q_6
PSD	10.3	248	2.7	291	-3.4	263	-6.4	284	-13.5	206	-18.7	236
MSA E	10.3	225	-7.0	286	-18.4	268	-24.1	286	-28.3	196	-34.9	238
MSA M	10.3	225	-10.8	287	-34.8	268	-23.7	290	-31.4	184	-32.5	235
MSA B	10.3	225	-17.2	285	-23.9	263	-16.5	287	-25.9	198	-27.5	235

cantilever oscillation signal [32]. Based on the equipartition theorem, for rectangular cantilevers in free air with constant cross section, the overall mean-square deflection of the cantilever caused by thermal vibrations \bar{y} depends on the absolute temperature T , cantilever spring constant k , and the deflection sensing method [31]. In particular, it has been shown that \bar{y} is the sum of the mean-square deflection of each vibration mode \bar{y}_i and can be expressed as

$$\bar{y} = \sum_{i=1}^{\infty} \bar{y}_i^2 = \frac{12k_B T}{k} \sum_{i=1}^{\infty} \frac{1}{\alpha_i^4} \quad (2)$$

where k_B is the Boltzmann constant and α_i are the solutions to the mode shape equation. It can be seen that the thermal vibration amplitude of higher eigenmodes rapidly decreases with α_i^{-4} . When the optical lever technique is employed, the thermal noise is determined by the slope of the cantilever which adds a scaling factor to (2) and causes nonvanishing thermal noise even during contact with a hard sample [31].

5) *Force Sensitivity*: Obtained by applying energy conservation principles and the virial theorem, widely used analytical formulas which describe average tip-sample force \bar{F}_{ts} [33] and average power dissipation \bar{P}_{ts} [34] for dynamic AFM have been derived

$$\bar{F}_{ts} = \frac{A_0 k}{2Q} \sqrt{1 - \left(\frac{A}{A_0}\right)^2} \quad (3)$$

$$\bar{P}_{ts} = \frac{k\omega}{2Q} (A A_0 \sin \phi - A^2). \quad (4)$$

These formulas are based on the assumption that an equivalent point mass spring damper system with stiffness k , quality factor Q , and resonance frequency ω is adequate to describe the cantilever dynamics and A_0 , A and ϕ denote free-air, in-contact amplitude, and phase, respectively. In particular, this model neglects the effect of higher (other) eigenmodes of the cantilever and assumes that constant hydrodynamic damping of the cantilever (Q factor is independent of tip-sample separation) [35]. As these equations were derived using a fundamental mode approximation, k is usually assumed to be equal to the static stiffness k_c . When these equations are used for higher modes, care must be taken to use the equivalent stiffness of the higher eigenmode which differs drastically

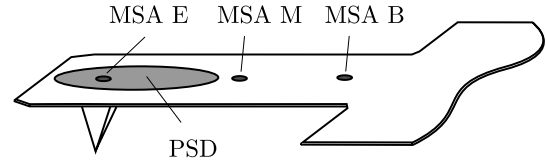


Fig. 2. Layout of the PSD and LDV measurements at different locations on the piezoelectric cantilever.

from k_c and also consider the effect of tip mass on the modal stiffness of higher modes [27].

C. Influence of the Deflection Sensor

The commonly used optical lever technique [36] measures the bending of the cantilever $y'(x) = dy(x)/dx$ rather than the displacement $y(x)$ by reflecting off a laser beam at a position x along the cantilever onto a position sensitive detector (PSD). The proportionality factor that relates bending and displacement for the static case was found for flat straight bar cantilevers [37] but has to be adapted for higher order bending modes [38].

Experimentally, the tip displacement $y_i(x)$ of the i th mode can be related to the PSD output $y_{\text{PSD},i}$ at that mode via the inverse optical lever sensitivity (invOLS) [39] of the i th mode of the PSD

$$y_i(x) = \text{invOLS}_i y_{\text{PSD},i}. \quad (5)$$

Conventionally, the invOLS is obtained from the linear contact regime of a quasi-static force curve [40] but due to the nature of slope detection, the calibration of the invOLS needs to be performed on the active eigenmode. In general, it was shown that optical lever sensitivity is increased for higher order eigenmodes due to the increasing slope of the mode shapes at the cantilever end [41]–[44].

To investigate the increase in sensitivity, the frequency response of a cantilever used in this work (see Section III-A) is measured with the optical lever method, using the PSD of an NT-MDT NTEGRA atomic force microscope, and with laser-doppler vibrometry (LDV), using a Polytec MSA-400 micro system analyser, at three different locations along the cantilever as indicated in Fig. 2. The results are shown in Fig. 3(a), where the measurements taken with the MSA-400 are scaled in

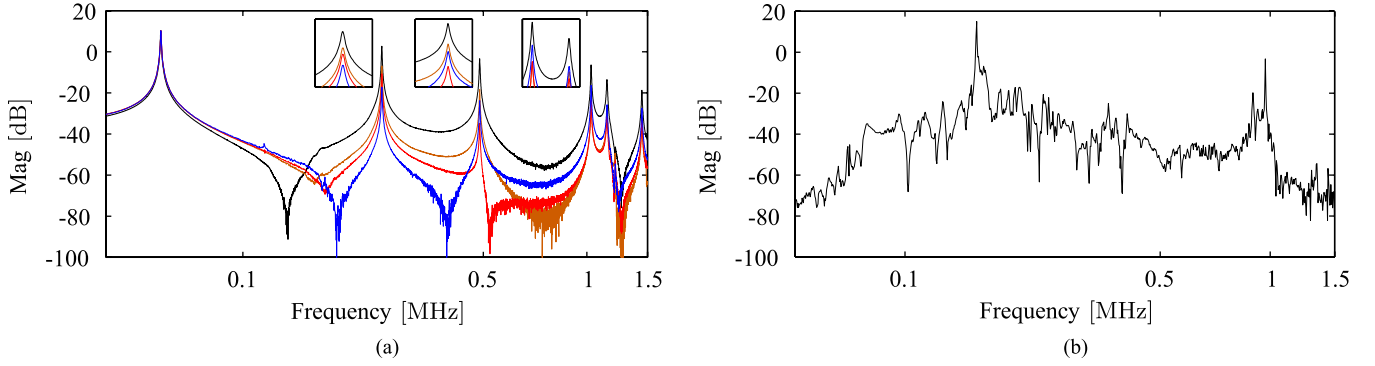


Fig. 3. (a) Frequency response data measured with the PSD (—) and using the MSA-400 at the piezoelectric cantilever end (MSA E (—), middle (MSA M) (—), and base (MSA B) (—)). (b) Frequency response data measured with the PSD (—) of an NT-MDT NSG01 base-excited cantilever.

magnitude to fit the measurement taken with the optical lever method to match on the first resonance mode. The magnitude response at each resonance frequency as well as the equivalent Q factor of each eigenmode are calculated by fitting a second-order transfer function and are shown in Table I. It can be observed that the optical lever measurement method leads to much larger magnitudes for higher eigenmodes than the true displacement measurements. This has the aforementioned positive impact on the sensitivity of measurements associated with these modes. Furthermore, we note that the frequencies of the zeros most prominently depend on the sensor position and while it appears that the Q factor is generally high for higher eigenmodes, it does not appear that the Q factor increases monotonically. This observation can be related to the deviation from a perfect rectangular cantilever without tip mass. As a comparison, the frequency response of a standard noncontact base-excited cantilever such as the NT-MDT NSG01 is shown in Fig. 3(b). While the first two resonant modes can be clearly identified, there exists no structured controller that would be capable of controlling those two modes simultaneously due to the high number of additional complex dynamics present. This fact emphasizes the need for integrated actuation.

III. MULTIMODE Q CONTROL

A. System Modeling

Taking a closer look at the cantilever subsystem of the AFM feedback loop highlighted in Fig. 1 provides more insight into the cantilever dynamics and the cantilever subsystem is shown in the block diagram in Fig. 4. Here, the cantilever is considered as a two-input (driving force and tip-sample force) single-output (deflection) system. The schematic and an image of the piezoelectrically actuated cantilever used in this work are shown in Fig. 5(a) and (b), respectively. When a voltage signal $V(t)$ is applied to the electrodes of the piezoelectric layer, it expands and contracts with a force $F_d(t)$ in the direction of the longitudinal axis of the cantilever. Since the cantilever is clamped at one end, this force creates a moment which translates into a displacement $y(t)$ at the free end. The tip-sample force $F_{ts}(d, t)$ acts on the cantilever tip and is collocated with the tip displacement.

When the cantilever is far away from the sample, the nonlinear block $F_{ts}(d, t) \equiv 0$ and the cantilever is oscillating

in free air with $y(t) = y_u(t)$. When the cantilever is engaged with the sample, the deflection becomes disturbed by $y_w(t)$, which is due to the nonlinear force input to $G_w(s)$. The two transfer functions $G_u(s)$ and $G_w(s)$ describe the input-output relationship from actuation input through the piezoelectric layer to cantilever displacement and from tip-sample disturbance input to cantilever displacement, respectively [45]. Since both transfer functions describe the same physical system, the location of the poles will be identical. However, the location of the zeros being a specification of the input-output behavior will differ yielding different transfer functions. Specifically, a cantilever with bonded piezoelectric transducer can be described by an infinite number of second-order modes of the form [21]

$$G_u(s) = \sum_{i=1}^{\infty} \frac{\alpha_i \omega_i^2}{s^2 + \frac{\omega_i}{Q_i} s + \omega_i^2}, \quad \omega_i, Q_i > 0, \quad \alpha_i \in \mathbb{R} \quad (6)$$

$$G_w(s) = \sum_{i=1}^{\infty} \frac{\beta_i \omega_i^2}{s^2 + \frac{\omega_i}{Q_i} s + \omega_i^2}, \quad \beta_i, \omega_i, Q_i > 0 \quad (7)$$

where each second-order mode is associated with a specific vibrational mode shape and is characterized in terms of the respective resonant frequency ω_i , quality factor Q_i , and gain α_i/β_i . $G_u(s)$ permits nonpositive α_i , whereas in $G_w(s)$ all β_i are positive leading to a collocated transfer function. This is expected since actuation and sensing take place at the same location on the cantilever. When these structures are modeled by considering only the first N modes, the resulting modeling error can be accommodated for by adding feedthrough terms D_u/D_w [46]

$$G_u(s) = \sum_{i=1}^N \frac{\alpha_i \omega_i^2}{s^2 + \frac{\omega_i}{Q_i} s + \omega_i^2} + D_u \quad (8)$$

$$G_w(s) = \sum_{i=1}^N \frac{\beta_i \omega_i^2}{s^2 + \frac{\omega_i}{Q_i} s + \omega_i^2} + D_w. \quad (9)$$

The transfer function G of a system is said to be NI if it is stable and satisfies the condition [47]

$$j[G(j\omega) - G^*(j\omega)] \geq 0 \quad \forall \omega > 0. \quad (10)$$

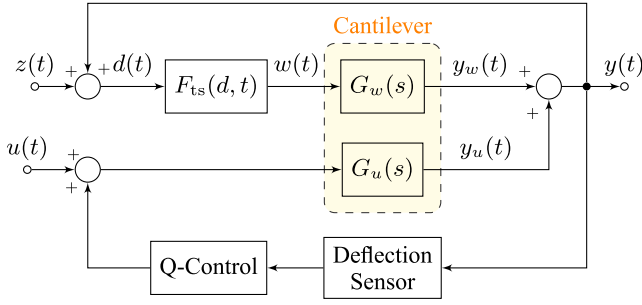


Fig. 4. Block diagram of the cantilever subsystem highlighting the feedback nature of the cantilever engaged with a sample.

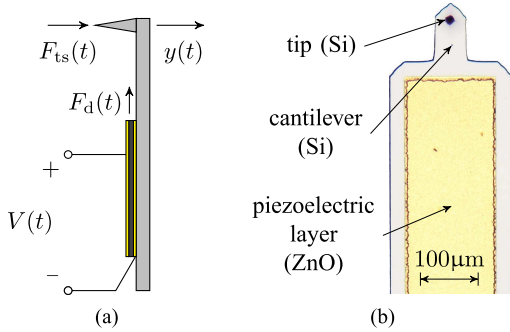


Fig. 5. (a) Simplified schematic (side view) and (b) image (top view) of the piezoelectric cantilever.

Moreover, G is strictly NI (SNI) if (10) holds with a strict inequality sign. It is straightforward to show that

$$j[G_w(j\omega) - G_w^*(j\omega)] = \sum_{i=1}^{\infty} \frac{2\beta_i \omega_i \omega \frac{1}{Q_i}}{(\omega_i^2 - \omega^2)^2 + \left(\omega_i \omega \frac{1}{Q_i}\right)^2} > 0 \quad (11)$$

with $\beta_i > 0$, $Q_i > 0$, and $\omega_i > 0$ and all the poles of (7) lie in the open half of the complex plane, thus rendering $G_w(s)$ SNI. Whether or not $G_u(s)$ is NI depends on the location of actuation and sensing. It could be seen in Fig. 3(a) that interlacing poles and zeros occur by moving the deflection sensor closer to the base. As the position of the laser spot is usually selected by the AFM user, no further conclusions are drawn on the NI property of $G_u(s)$ when using the optical lever method.

B. Positive Position Feedback Controller

The positive position feedback (PPF) controller [48] can be used to control M modes of the microcantilever and is of the form

$$K_{\text{PPF}}(s) = \sum_{i=1}^M \frac{\gamma_{c,i}}{s^2 + 2\zeta_{c,i}\omega_{c,i}s + \omega_{c,i}^2} \quad (12)$$

with $\gamma_{c,i}$, $\zeta_{c,i}$, and $\omega_{c,i}$ being the tunable controller parameters. From its structure, it can be verified immediately that it satisfies the SNI property if $\gamma_{c,i}$, $\zeta_{c,i}$, and $\omega_{c,i} > 0$. The NI lemma states that the positive feedback interconnection of an SNI plant and an NI controller is internally stable if and only if the dc-gain condition $G(0)K(0) < 1$ is satisfied [49].

For systems with mixed NI and finite-gain properties, the stability of the positive interconnection can also be shown using the notion of dissipativity [50].

If the plant cannot be guaranteed to be NI, a PPF controller design method can be derived as follows. Consider the single-mode approximation of the cantilever by setting $i = 1$ in (8) in the time-domain

$$\ddot{x}(t) + \frac{\omega}{Q}\dot{x}(t) + \omega^2 x(t) = \alpha \omega^2 u(t) \quad (13)$$

$$y(t) = \alpha \omega^2 x(t) + Du(t) \quad (14)$$

with a nonzero feedthrough term D and the PPF controller

$$\ddot{x}_c(t) + 2\zeta_c \omega_c \dot{x}_c(t) + \omega_c^2 x_c(t) = \gamma_c y(t) \quad (15)$$

$$u(t) = \gamma_c x_c(t). \quad (16)$$

The closed-loop system is obtained by substituting (16) in (13) and (14), (16) in (15) and defining $z = [x(t) \ x_c(t)]^T$, which yields

$$\ddot{z} + \underbrace{\begin{bmatrix} \frac{\omega}{Q} & 0 \\ 0 & 2\zeta_c \omega_c \end{bmatrix}}_{E=E^T} \dot{z} + \underbrace{\begin{bmatrix} \omega^2 & -\gamma_c \alpha \omega^2 \\ -\gamma_c \alpha \omega^2 & \omega_c^2 - \gamma_c D \gamma_c \end{bmatrix}}_{K=K^T} z = 0. \quad (17)$$

By choosing the state space variables $Z = [z \ \dot{z}]^T$, (17) can be rewritten as

$$\dot{Z} = \begin{bmatrix} 0 & I \\ -K & -E \end{bmatrix} Z \quad (18)$$

where I is the identity matrix. Assuming $E > 0$ and $K > 0$, the Lyapunov stability of (18) can be shown with [21]

$$V(Z) = Z^T \begin{bmatrix} K + \tau I & \tau I \\ \tau I & I \end{bmatrix} Z \geq 0 \quad (19)$$

$$\dot{V}(Z) = Z^T \begin{bmatrix} -2\tau K & 0 \\ 0 & 2(\tau I - E) \end{bmatrix} Z < 0 \quad (20)$$

where $0 \leq \tau \leq \lambda_{\min}(E)$. For E to be positive definite, all eigenvalues must be positive and since E is in diagonal form

$$E > 0 \iff Q > 0, \ \omega > 0, \ \zeta_c > 0, \ \omega_c > 0. \quad (21)$$

For K to be positive definite, the definition in (17) can be rewritten as

$$\begin{bmatrix} \omega^2 & -\gamma_c \alpha \omega^2 \\ -\gamma_c \alpha \omega^2 & \omega_c^2 \end{bmatrix} - \begin{bmatrix} 0 \\ \gamma_c \end{bmatrix} D \begin{bmatrix} 0 & \gamma_c \end{bmatrix} > 0. \quad (22)$$

Applying the Schur-complement yields a linear matrix inequality (LMI) in the variables γ_c and ω_c^2

$$\begin{bmatrix} \omega^2 & -\gamma_c \alpha \omega^2 & 0 \\ -\gamma_c \alpha \omega^2 & \omega_c^2 & \gamma_c \\ 0 & \gamma_c & D^{-1} \end{bmatrix} > 0. \quad (23)$$

Therefore, the conditions (23) and $\zeta_c > 0$ from (21) which determine the stability of the PPF controller in positive feedback with a single-mode plant can be written as an LMI which is a convex problem [51]. Determining the stability of such a feedback system is a convex optimization problem and is also known as the feasibility problem [52]. Moreover, the convex constraint can be exploited for the controller design to ensure closed-loop stability, which will be discussed in the following section.

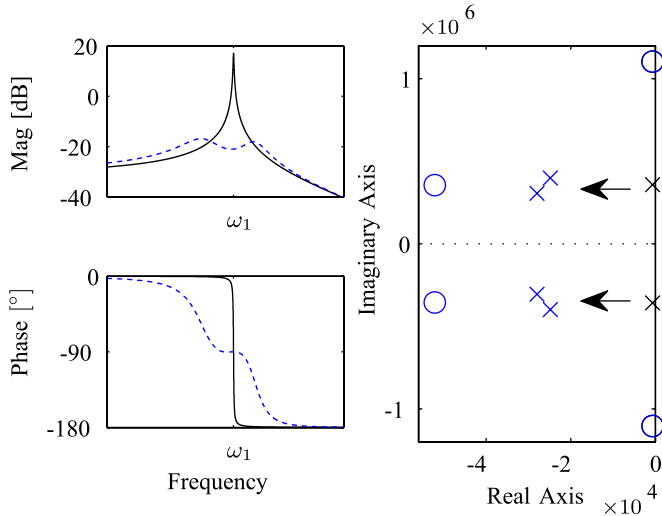


Fig. 6. Left: Bode plot of the first mode of open-loop (—) and closed-loop system with H_∞ norm minimization PPF controller (---). Right: Pole-zero map of open-loop (\times, \circ) and closed-loop (\times, \circ) system.

C. Controller Design

Controller design is carried out for each eigenmode of the cantilever individually by appropriately setting i in (8) and (12). To achieve maximum damping of an eigenmode, the controller design is formulated as an optimization problem of the form

$$\begin{aligned} \min_{\gamma_c, \zeta_c, \omega_c} \quad & \|G_{cl}(j\omega)\|_\infty \\ \text{s.t.} \quad & 0 < \zeta_c \leq \zeta_{c,\max} \\ & 0 < \omega_c \leq \omega_{c,\max} \\ & \begin{bmatrix} \omega^2 & -\gamma_c \alpha \omega^2 & 0 \\ -\gamma_c \alpha \omega^2 & \omega_c^2 & \gamma_c \\ 0 & \gamma_c & D^{-1} \end{bmatrix} > 0 \end{aligned} \quad (24)$$

where the cost function is the H_∞ -norm of the closed-loop system

$$\|G_{cl}(j\omega)\|_\infty = \max_{\omega} |G_{cl}(j\omega)| \quad (25)$$

which corresponds to the peak gain of the frequency response. The constraints $\zeta_{c,\max}$ and $\omega_{c,\max}$ correspond to restrictions on the implementation. Notice that while minimizing the H_∞ -norm of an affine function is a convex problem [53], the objective function in this case is nonlinear in the optimization variables γ_c, ζ_c and ω_c^2 , hence rendering the overall problem nonconvex. Here, we chose to minimize the H_∞ -norm of the closed-loop system as it resembles minimizing the maximum peak in the frequency response which corresponds to the resonance peak. Other choices are possible such as minimizing the H_2 -norm which also has a control system interpretation in terms of minimizing the output variance of the system when excited by a white noise input signal [53].

Simulation results are presented in Fig. 6. The optimization routine places the closed-loop poles deeper in the left half of the complex plane, leading to a damped frequency response. However, the separation of closed-loop poles yields two peaks

around the resonance frequency which is disadvantageous if AFM scans were to be obtained with that resonant mode.

In order to design a controller for an eigenmode to be suitable for AFM imaging, a different approach has to be taken that exactly places the real part of the closed-loop poles $\Re(p_{i,cl})$ at a desired location $p_{i,des}$ by finding a solution to the optimization problem of the form

$$\begin{aligned} \min_{\gamma_c, \zeta_c, \omega_c} \quad & J(\gamma_c, \zeta_c, \omega_c) \\ \text{s.t.} \quad & 0 < \zeta_c \leq \zeta_{c,\max} \\ & 0 < \omega_c \leq \omega_{c,\max} \\ & \begin{bmatrix} \omega^2 & -\alpha \omega^2 \gamma_c & 0 \\ -\gamma_c \alpha \omega^2 & \omega_c^2 & \gamma_c \\ 0 & \gamma_c & D^{-1} \end{bmatrix} > 0. \end{aligned} \quad (26)$$

Here, the cost function

$$J(\gamma_c, \zeta_c, \omega_c) = \sum_{i=1}^4 (p_{i,des} - \Re(p_{i,cl}))^2 + \sum_{i=3}^4 |p_{i,cl} - p_{i-2,cl}|^2 \quad (27)$$

penalizes the difference between the desired and actual pole locations and between poles that correspond to the same open-loop poles if the closed-loop poles are ordered in descending order. The method ensures a defined shape of the resonance peak which is suitable for AFM imaging. Unlike the nonlinear relationship of feedback gain and resulting Q factor using time-delay Q control [20], this approach has a inverse proportional relationship between the desired effective Q factor Q^* and the desired real part of the closed-loop poles via the second-order approximation

$$\Re(p_i) = \frac{\omega_2}{-2Q^*}. \quad (28)$$

Notice that the objective function is nonlinear in the optimization variables γ_c, ζ_c , and ω_c^2 , hence rendering the overall problem nonconvex. However, in practice, initialization of the optimization problem with a feasible set calculated from (23) and (21) yields good convergence and damping performance as can be seen in the simulated example in Fig. 7. It can be seen that closed-loop poles do not separate resulting in an adequately shaped resonance peak, suitable for AFM imaging.

D. Stability Properties

The sum of the single-mode PPF controllers resulting from the above design procedures yields a multimode PPF controller

$$K(s) = \sum_{i=1}^2 \frac{\gamma_{c,i}}{s^2 + 2\zeta_{c,i}\omega_{c,i}s + \omega_{c,i}^2} \quad (29)$$

which completely damps nondriven eigenmodes and suitably lowers the Q factor of the driven eigenmode. Fig. 8 shows the frequency response of the resulting controller for a cantilever with interlacing poles and zeros up to the second eigenmode, such as in Fig. 3(a). It can be observed that the control energy is focused around the resonance peaks and the controller gain rolls off quickly at

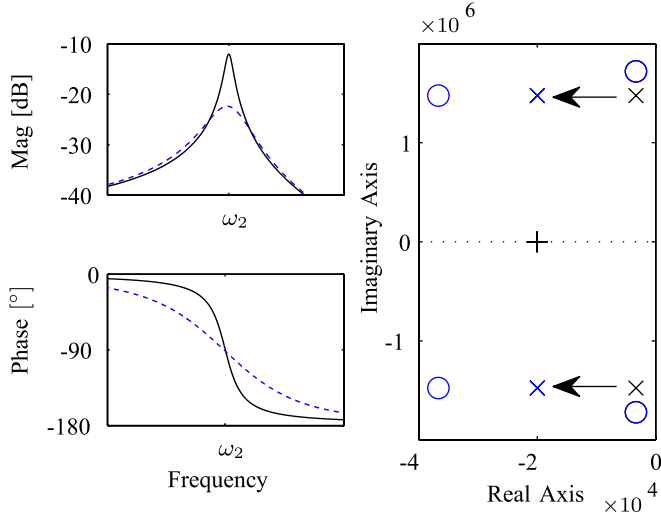


Fig. 7. Left: Bode plot of the second mode of open-loop (—) and closed-loop system with pole optimization PPF controller (—). Right: Pole-zero map of desired pole location (+), open-loop (×, ○) and closed-loop (×, ○) system.

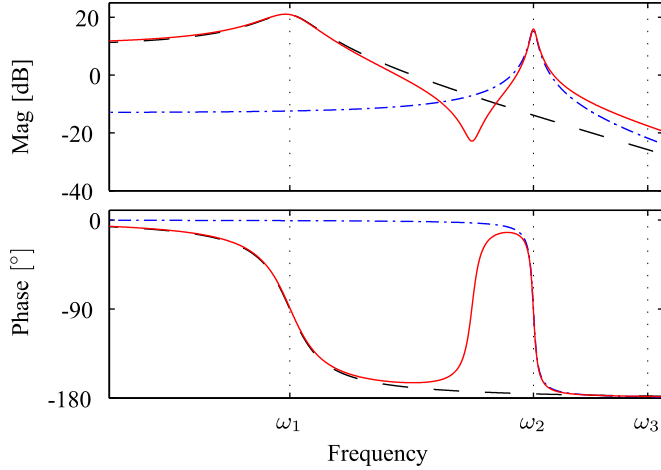


Fig. 8. Bode plot of first eigenmode PPF controller (—), second eigenmode PPF controller (— · —), and multimode Q controller (—).

higher frequencies, benefiting the nonexcitement of higher-order eigenmodes. At the resonance frequencies, the phase crosses -90° , which resembles velocity feedback at that frequency, resulting in a reduction in the Q factor. Furthermore, it can be seen that the phase remains within the bounds $[0^\circ, -180^\circ]$, which is a property of single input single output NI systems. The positive feedback connection of such an SNI controller with an NI plant as shown in Fig. 3(a) is guaranteed to be robustly stable with a gain margin of $G_m = (G_i(0)K_i(0))^{-1}$ corresponding to the dc-gain condition [49].

If the transfer function of a single-mode $G_j(s)$ of the cantilever violates the NI property because $\alpha_j < 0$ and therefore no complex conjugate zero pair lies between adjacent complex conjugate pole pairs (compare Fig. 9), the above design procedure to lower the Q factor of the respective mode will yield a PPF controller $K_j(s)$ with $\gamma_{c,j} < 0$. Note that in this case $-G_j(s)$ and $-K_j(s)$ satisfy the SNI property and the poles of their positive feedback connection

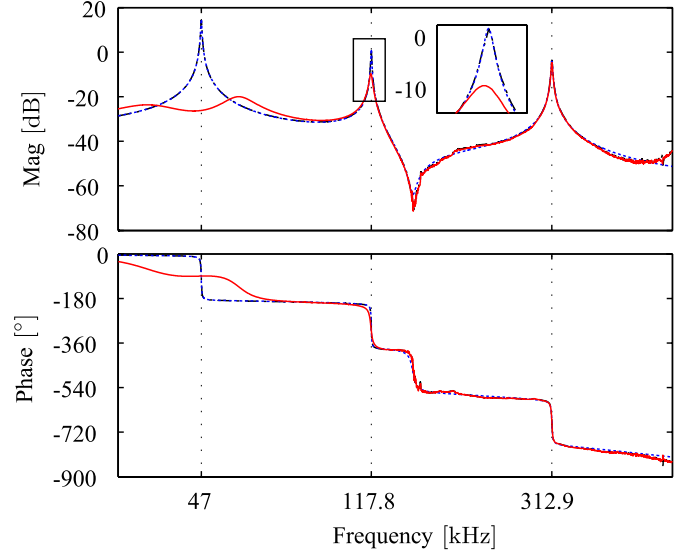


Fig. 9. Bode plot showing the measured open-loop frequency response (— · —), its identified model (— · —), and the measured closed-loop frequency response (—) for imaging on the second eigenmode.

TABLE II
PARAMETERS OF THE FIXED STRUCTURE MODEL

Mode	f_i [kHz]	Q_i	α_i [$\mu\text{m}/\text{V}$]
1	47.0	212	0.0275
2	117.8	227	-0.0045
3	312.9	177	-0.0028

$1 - (-G_j(s))(-K_j(s))$ are the same as $1 - (G_j(s))(K_j(s))$, which is therefore robustly stable if the dc-gain condition $G_j(0)K_j(0) < 1$ is satisfied.

For the overall multimode Q controller (with mixed NI property) in positive feedback with the multimode plant (with mixed NI property), stability analysis is carried out using the Nyquist criterion of the open-loop chain $-K(s)G(s)$; the stability margins are stated in Section IV-A. In addition, the gain of the multimode PPF Q controller rolls off quickly for higher frequencies benefiting the nonexcitement of unmodeled higher order eigenmodes of the cantilever.

IV. EXPERIMENTAL RESULTS

A. System Identification

The AFM cantilever used in this work is the piezoelectric self-actuated silicon microcantilever described in Section III-A. Frequency response data were obtained by performing a sinusoidal sweep using a Zurich Instruments HF2LI lock-in amplifier. Using frequency domain subspace identification [54], a sixth-order state space model was obtained for the first three eigenmodes of the cantilever. From the model, the fixed structure form (8) for $n = 3$ is calculated with parameters shown in Table II.

Following the design procedures discussed in Section III-C, the multimode controllers were implemented on a field-programmable analog array (FPAA). The Anadigm AN221E04 FPAA offers sufficient bandwidth and provides enough flexibility through configurable analog modules to control resonant

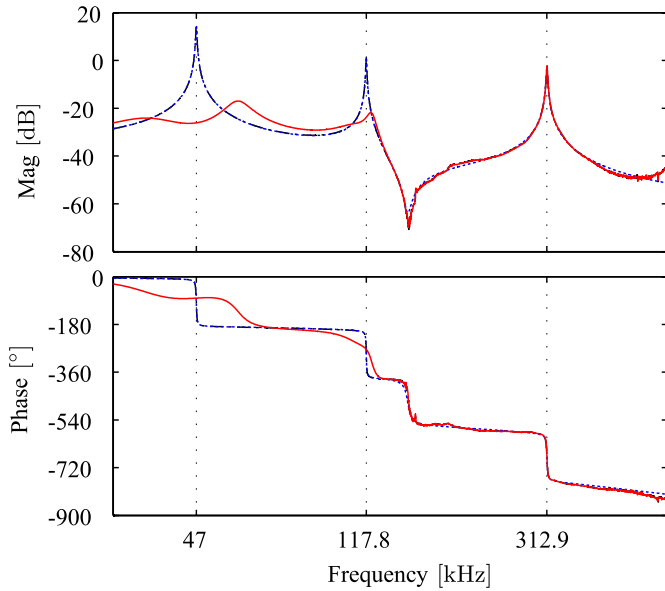


Fig. 10. Bode plot showing the measured open-loop frequency response (---), its identified model (---), and the measured closed-loop frequency response (—) for imaging on the third eigenmode.

modes up to 400 kHz. The measured open-loop frequency response along with its identified model and the measured closed-loop frequency responses are shown in Figs. 9 and 10. Note that this specific cantilever does not show interlacing poles and zeros up to the second eigenmode; however, the design procedure yields a PPF controller which performs equally well.

To demonstrate imaging on the second eigenmode, the first resonance was heavily damped by 34 dB. In addition, the Q factor of the second eigenmode was set to $Q_2^* \approx 60$ resulting in 11 dB damping while leaving the third resonance unaffected. The measured frequency response is shown in Fig. 9. To demonstrate imaging on the third eigenmode, the first and second resonances were heavily damped by 34 and 24 dB, respectively, in order to render the third resonance dominant. The measured frequency response is shown in Fig. 10. The stability margins extracted from the measured open-loop chain $-K(s)G(s)$ (not shown) for the two closed-loop systems are $G_m = 25.4$ dB at 106 kHz for the system in Fig. 9 and $G_m = 18.7$ dB at 315 kHz for the system in Fig. 10. As will be discussed, both systems yield an increased effective cantilever bandwidth and therefore improved image quality.

B. Imaging Stability

In order to achieve stable imaging conditions on the higher eigenmode, the lower nondriven eigenmodes need to be damped as much as possible to prevent spontaneous excitation through the nonlinear tip-sample force. This is demonstrated in Fig. 11 where the cantilever is excited at its third resonance frequency and tapping a TGZ1 calibration grating at a setpoint of 88%. In Fig. 11(a) and (c), the uncontrolled lower eigenmodes are spontaneously excited, leading to unstable cantilever oscillations. The contribution of the lower two flexural

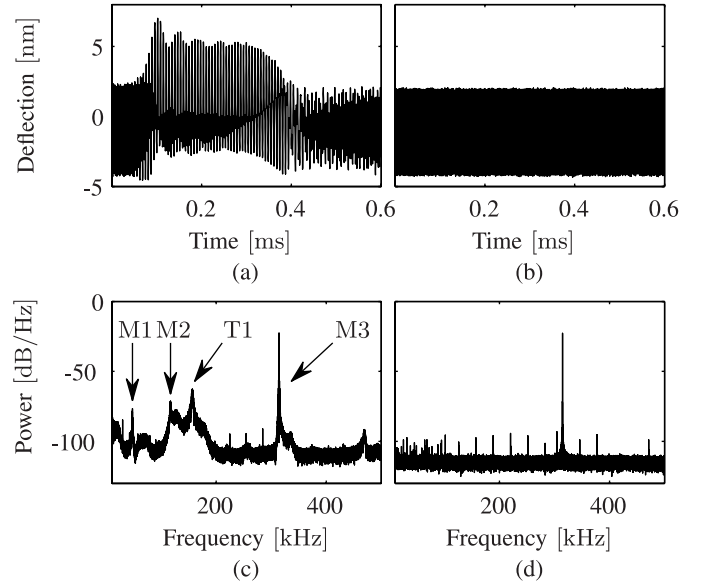


Fig. 11. Time-domain deflection signal of the cantilever tapping at the third eigenmode for (a) open-loop and (b) using multimode Q control at a setpoint of 88%. Power spectral density estimate of the deflection signal for (c) open-loop and (d) using multimode Q control.

eigenmodes M1 and M2 as well as a lower torsional mode T1 is clearly visible in the power spectral density estimate. In Fig. 11(b) and (d), the lower eigenmodes are damped thus preventing excitation for the same setpoint. The estimate was obtained from the time-domain deflection signal sampled at 5 MHz using Welch's overlapped segment averaging estimator with eight sections windowed with the Hamming window and an overlap of 50%.

C. AFM Experiments

This section shows how imaging on higher order eigenmodes and/or additionally lowering the quality factor increases the effective cantilever bandwidth, which leads to improved topography tracking. As a consequence of lowering the Q factor, the drive voltage is adapted for each experiment in order to maintain the same free air amplitude. Furthermore, according to (3), the imaging setpoint needs to be adapted as a consequence of the higher dynamic stiffness of the higher order mode and lower Q factor in order to maintain an equal average tip-sample force and therefore comparable imaging conditions. The nanopositioner used in this work is a NT-MDT piezoelectric tube scanner with xyz capacitive displacement sensors, 100 μm lateral range, 10 μm vertical range, and a z -axis resonance frequency of approximately 700 Hz. A conservative approximation of its z -axis bandwidth [55] evaluates to approximately 125 Hz. As the manufacturer does not provide noise specifications of the photo diode sensor, a thermal noise spectrum was obtained by recording time-domain deflection data in free-air and calculating a power spectral density estimate using Welch's method (not shown). From the estimate, a noise density of $1.2 \mu\text{V}/\sqrt{\text{Hz}}$ was calculated, which equates to approximately $720 \text{ fm}/\sqrt{\text{Hz}}$ using the invOLS of the fundamental mode and approximately $20 \text{ fm}/\sqrt{\text{Hz}}$ using the invOLS of the third mode.

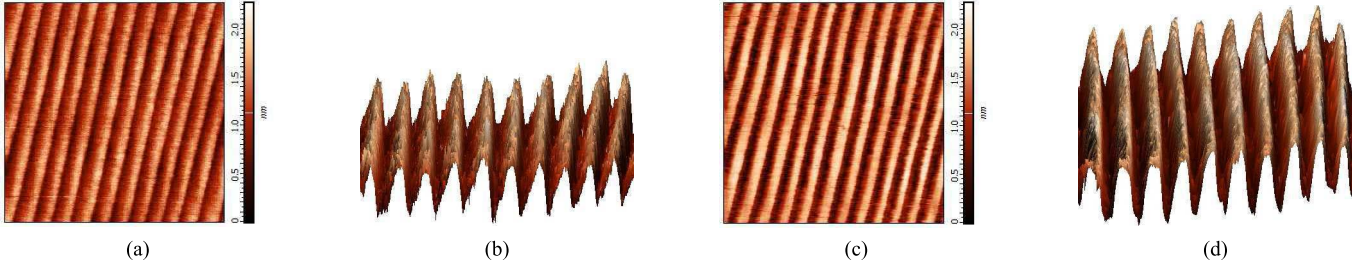


Fig. 12. (a) and (b) Scan on the first eigenmode without Q control. (c) and (d) Scan on the third eigenmode with multimode Q control. (a) Mode 1: 2-D image. (b) Mode 1: 3-D image. (c) Mode 3: 2-D image. (d) Mode 3: 3-D image.

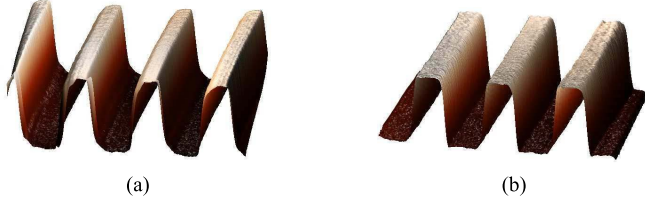


Fig. 13. (a) Scan on the first eigenmode at $156.3 \mu\text{m/s}$ without Q control. (b) Scan on the second eigenmode at $156.3 \mu\text{m/s}$ with multimode Q control. (a) Mode 1: 3-D image. (b) Mode 2: 3-D image.

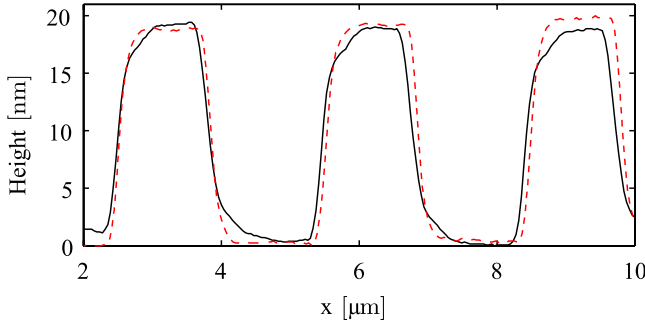


Fig. 14. Cross-section analysis of image obtained on first eigenmode without Q control (—) [compare Fig. 13(a)] and of image obtained on second eigenmode with multimode Q control (---) [compare Fig. 13(b)].

1) *Imaging of TGZ1 Calibration Grating:* Scans of an NT-MDT TGZ1 calibration grating were obtained on an NT-MDT NTEGRA AFM. The sample has periodic features of heights $h = 21.6 \pm 1.5 \text{ nm}$ and was scanned at a speed of $156.3 \mu\text{m/s}$ at an area of $10 \mu\text{m} \times 10 \mu\text{m}$ with a free-air amplitude of $A_0 \approx 100 \text{ nm}$.

For the cantilever used in this work with a fundamental resonance frequency of 47 kHz and a native quality factor of $Q_1 = 212$, the effective cantilever bandwidth according to (1) is $f_{c,1} \approx 111 \text{ Hz}$. When imaging is performed on the fundamental mode without Q control, the low cantilever bandwidth only permits a low z -axis feedback gain and therefore poor topography tracking as can be seen in Fig. 13(a) and in the cross-section analysis in Fig. 14. By employing multimode Q control to completely damp the first eigenmode and additionally lowering the Q factor of the second eigenmode as shown in Fig. 9, the effective cantilever bandwidth when imaging on the second eigenmode is increased to $f_{c,2} \approx 982 \text{ Hz}$. The imaging results are shown

in Figs. 13(b) and 14. Due to the increased effective cantilever bandwidth, the z -axis feedback gain could be increased, which leads to more accurate tracking of the rectangular sample features.

2) *Imaging of Monolayer Silicon Carbide:* An NT-MDT silicon carbide (SiC) calibration sample with features of monolayer high steps of $h = 1.5 \text{ nm}$ corresponding to the lattice constant of the 6H-SiC crystal in the $[0001]$ direction was imaged. Due to the small nanometer features, the scan area was chosen to be $2 \mu\text{m} \times 2 \mu\text{m}$, the scan speed was set to $4.05 \mu\text{m/s}$, and a small free-air amplitude of $A_0 \approx 10 \text{ nm}$ had to be employed. The 2-D and 3-D images obtained on the fundamental eigenmode without Q control are shown in Fig. 12(a) and (b), respectively. After the sample tilt was accounted for by removing a fitted plane, the observed features appear as peaks rather than as terraces. By employing multimode Q control to completely damp the first and second eigenmodes in order to render the third mode dominant, the system shown in Fig. 10 yields an effective cantilever bandwidth of $f_{c,3} \approx 884 \text{ Hz}$. As a consequence, the z -axis feedback gain could be increased by a factor of three, yielding a much higher contrast, which can be observed by comparing the 2-D and 3-D images shown in Fig. 12. Also, note that the increased OLS (compare Section II-C) of the third mode yields less noise for small free air amplitudes than the fundamental mode, which can also be seen in Fig. 12. Further we note that, when operating on the first eigenmode, a meaningful image could be obtained only by lowering the set point amplitude to about 40% of the free air amplitude in contrast to 88% when the cantilever is oscillated at its third eigenmode. This is explained from (3), which states that the tip-sample force scales with the dynamic stiffness of the eigenmode and, as in this case when free-air amplitudes are kept constant, allows an increase in set point amplitude in order to maintain equal tip-sample forces.

V. CONCLUSION

When a cantilever with integrated actuation, such as with a bonded piezoelectric layer, is used for tapping-mode atomic force microscopy, the transfer function from actuation voltage to cantilever deflection shows a well-defined magnitude and phase response. On this basis, controllers to regulate the Q factor of individual resonant modes can be derived to achieve excellent performance by relying on PPF. Moreover, if collocated actuation and sensing can be achieved, these

controllers have guaranteed stability properties compared with the standard time-delay method to change the cantilever quality factor. The advantage of controlling resonant modes becomes apparent when higher flexural eigenmodes of the microcantilever are to be used in tapping-mode AFM. Not only do these higher eigenmodes exhibit faster transient response times, which allows a higher z -axis feedback gain and, in turn, improved image quality, but they also offer varying Q factors, increased dynamic stiffnesses, and an increased OLS in air. However, if preceding nondriven eigenmodes are not adequately damped, imaging on higher eigenmodes may lead to poor imaging stability. The proposed control method can be used to heavily damp preceding eigenmodes or to change the on-mode Q factor as desired. Therefore, a single cantilever combined with multimode Q control can serve as a flexible force sensor for different sample materials.

In future work, Ruppert and Moheimani [56], [57] aim to further develop the self-sensing scheme for higher order eigenmodes that may guarantee collocated actuation and sensing and therefore guaranteed stability of PPF to control the cantilever Q factor. Moreover, as multiple ways of bimodal and trimodal multifrequency AFM methods [58] gain more and more importance, the ability to control multiple eigenmodes during such experiments can undoubtedly be of further benefit [23].

ACKNOWLEDGMENT

This research was performed in the Laboratory for Dynamics and Control of Nanosystems at The University of Newcastle, Callaghan, NSW, Australia.

REFERENCES

- [1] G. Binnig, C. F. Quate, and C. Gerber, "Atomic force microscope," *Phys. Rev. Lett.*, vol. 56, pp. 930–933, Mar. 1986.
- [2] T. R. Albrecht, P. Grütter, D. Horne, and D. Rugar, "Frequency modulation detection using high- Q cantilevers for enhanced force microscope sensitivity," *J. Appl. Phys.*, vol. 69, no. 2, pp. 668–673, 1991.
- [3] Y. Martin, C. C. Williams, and H. K. Wickramasinghe, "Atomic force microscope–force mapping and profiling on a sub 100-Å scale," *J. Appl. Phys.*, vol. 61, no. 10, pp. 4723–4729, 1987.
- [4] A. Raman, J. Melcher, and R. Tung, "Cantilever dynamics in atomic force microscopy," *Nano Today*, vol. 3, nos. 1–2, pp. 20–27, 2008.
- [5] S. Kawai, S.-I. Kitamura, D. Kobayashi, S. Meguro, and H. Kawakatsu, "An ultrasmall amplitude operation of dynamic force microscopy with second flexural mode," *Appl. Phys. Lett.*, vol. 86, no. 19, p. 193107, 2005.
- [6] S. Kawai and H. Kawakatsu, "Atomically resolved dynamic force microscopy operating at 4.7 MHz," *Appl. Phys. Lett.*, vol. 88, no. 13, p. 133103, 2006.
- [7] Y. Sugimoto, S. Innami, M. Abe, Ó. Custance, and S. Morita, "Dynamic force spectroscopy using cantilever higher flexural modes," *Appl. Phys. Lett.*, vol. 91, no. 9, p. 093120, 2007.
- [8] S. Rast, C. Wattinger, U. Gysin, and E. Meyer, "The noise of cantilevers," *Nanotechnology*, vol. 11, no. 3, p. 169, 2000.
- [9] O. Pfeiffer *et al.*, "Using higher flexural modes in non-contact force microscopy," *Appl. Surf. Sci.*, vol. 157, no. 4, pp. 337–342, 2000.
- [10] S. Rast, C. Wattinger, U. Gysin, and E. Meyer, "Dynamics of damped cantilevers," *Rev. Sci. Instrum.*, vol. 71, no. 7, pp. 2772–2775, 2000.
- [11] R. W. Stark, T. Drobek, and W. M. Heckl, "Tapping-mode atomic force microscopy and phase-imaging in higher eigenmodes," *Appl. Phys. Lett.*, vol. 74, no. 22, pp. 3296–3298, 1999.
- [12] A. Ulcinas and V. Snitka, "Intermittent contact AFM using the higher modes of weak cantilever," *Ultramicroscopy*, vol. 86, nos. 1–2, pp. 217–222, 2001.
- [13] J. Mertz, O. Marti, and J. Mlynek, "Regulation of a microcantilever response by force feedback," *Appl. Phys. Lett.*, vol. 62, no. 19, pp. 2344–2346, 1993.
- [14] T. Sulchek, R. Hsieh, J. D. Adams, G. G. Yaralioglu, S. C. Minne, and C. F. Quate, "High-speed tapping mode imaging with active Q control for atomic force microscopy," *Appl. Phys. Lett.*, vol. 76, no. 11, pp. 1473–1475, 2000.
- [15] A. D. L. Humphris, A. N. Round, and M. J. Miles, "Enhanced imaging of DNA via active quality factor control," *Surf. Sci.*, vol. 491, no. 3, pp. 468–472, 2001.
- [16] T. R. Rodríguez and R. García, "Theory of Q control in atomic force microscopy," *Appl. Phys. Lett.*, vol. 82, no. 26, pp. 4821–4823, 2003.
- [17] J. Kokavecz, Z. L. Horváth, and Á. Mechler, "Dynamical properties of the Q -controlled atomic force microscope," *Appl. Phys. Lett.*, vol. 85, no. 15, pp. 3232–3234, 2004.
- [18] M. Fairbairn and S. O. R. Moheimani, "Resonant control of an atomic force microscope micro-cantilever for active Q control," *Rev. Sci. Instrum.*, vol. 83, no. 8, pp. 083708-1–083708-9, 2012.
- [19] H. Hölscher, D. Ebeling, and U. D. Schwarz, "Theory of Q -controlled dynamic force microscopy in air," *J. Appl. Phys.*, vol. 99, no. 8, p. 084311, 2006.
- [20] H. Hölscher and U. D. Schwarz, "Theory of amplitude modulation atomic force microscopy with and without Q -control," *Int. J. Non-Linear Mech.*, vol. 42, no. 4, pp. 608–625, 2007.
- [21] S. O. R. Moheimani and A. J. Fleming, *Piezoelectric Transducers for Vibration Control and Damping*. London, U.K.: Springer-Verlag, 2006.
- [22] M. G. Ruppert, M. W. Fairbairn, and S. O. R. Moheimani, "Multi-mode resonant control of a microcantilever for atomic force microscopy," in *Proc. IEEE/ASME Int. Conf. Adv. Intell. Mechatronics*, Wollongong, NSW, Australia, Jul. 2013, pp. 77–82.
- [23] M. G. Ruppert and S. O. R. Moheimani, "Multi-mode Q control in multifrequency atomic force microscopy," in *Proc. ASME Int. Design Eng. Tech. Conf. Comput. Inf. Eng. Conf. (IDETC/CIE)*, Boston, MA, USA, Aug. 2015.
- [24] T. Ando, T. Uchihashi, and T. Fukuma, "High-speed atomic force microscopy for nano-visualization of dynamic biomolecular processes," *Prog. Surf. Sci.*, vol. 83, nos. 7–9, pp. 337–437, 2008.
- [25] A. Volodin and C. Van Haesendonck, "Low temperature force microscopy based on piezoresistive cantilevers operating at a higher flexural mode," *Appl. Phys. A*, vol. 66, no. 1, pp. S305–S308, 1998.
- [26] M. Hoummady and E. Farnault, "Enhanced sensitivity to force gradients by using higher flexural modes of the atomic force microscope cantilever," *Appl. Phys. A*, vol. 66, no. 1, pp. S361–S364, 1998.
- [27] J. Melcher, S. Hu, and A. Raman, "Equivalent point-mass models of continuous atomic force microscope probes," *Appl. Phys. Lett.*, vol. 91, no. 5, p. 053101, 2007.
- [28] J. R. Lozano, D. Kiracofe, J. Melcher, R. García, and A. Raman, "Calibration of higher eigenmode spring constants of atomic force microscope cantilevers," *Nanotechnology*, vol. 21, no. 46, p. 465502, 2010.
- [29] J. E. Sader, J. W. M. Chon, and P. Mulvaney, "Calibration of rectangular atomic force microscope cantilevers," *Rev. Sci. Instrum.*, vol. 70, no. 10, pp. 3967–3969, 1999.
- [30] J. L. Hutter and J. Bechhoefer, "Calibration of atomic-force microscope tips," *Rev. Sci. Instrum.*, vol. 64, no. 7, pp. 1868–1873, 1993.
- [31] H.-J. Butt and M. Jaschke, "Calculation of thermal noise in atomic force microscopy," *Nanotechnology*, vol. 6, no. 1, p. 1, 1995.
- [32] Y. Gan, "Atomic and subnanometer resolution in ambient conditions by atomic force microscopy," *Surf. Sci. Rep.*, vol. 64, no. 3, pp. 99–121, 2009.
- [33] Á. San Paulo and R. García, "Tip-surface forces, amplitude, and energy dissipation in amplitude-modulation (tapping mode) force microscopy," *Phys. Rev. B*, vol. 64, p. 193411, Oct. 2001.
- [34] B. Anczykowski, B. Gotsmann, H. Fuchs, J. P. Cleveland, and V. B. Elings, "How to measure energy dissipation in dynamic mode atomic force microscopy," *Appl. Surf. Sci.*, vol. 140, nos. 3–4, pp. 376–382, 1999.
- [35] R. García and Á. San Paulo, "Attractive and repulsive tip-sample interaction regimes in tapping-mode atomic force microscopy," *Phys. Rev. B*, vol. 60, pp. 4961–4967, Aug. 1999.
- [36] G. Meyer and N. M. Amer, "Novel optical approach to atomic force microscopy," *Appl. Phys. Lett.*, vol. 53, no. 12, pp. 1045–1047, 1988.
- [37] S. A. C. Gould *et al.*, "The atomic force microscope: A tool for science and industry," *Ultramicroscopy*, vol. 33, no. 2, pp. 93–98, 1990.
- [38] E. Meyer, H. J. Hug, and R. Bennewitz, *Scanning Probe Microscopy*. Berlin, Germany: Springer-Verlag, 2004.

- [39] R. Proksch, T. E. Schäffer, J. P. Cleveland, R. C. Callahan, and M. B. Viani, "Finite optical spot size and position corrections in thermal spring constant calibration," *Nanotechnology*, vol. 15, no. 9, p. 1344, 2004.
- [40] H.-J. Butt, B. Cappella, and M. Kappl, "Force measurements with the atomic force microscope: Technique, interpretation and applications," *Surf. Sci. Rep.*, vol. 59, nos. 1–6, pp. 1–152, 2005.
- [41] U. Rabe, K. Janser, and W. Arnold, "Vibrations of free and surface-coupled atomic force microscope cantilevers: Theory and experiment," *Rev. Sci. Instrum.*, vol. 67, no. 9, pp. 3281–3293, 1996.
- [42] M. Hoummady, E. Farnault, T. Yahiro, and H. Kawakatsu, "Simultaneous optical detection techniques, interferometry, and optical beam deflection for dynamic mode control of scanning force microscopy," *J. Vac. Sci. Technol. B*, vol. 15, no. 4, pp. 1539–1542, 1997.
- [43] T. E. Schäffer and H. Fuchs, "Optimized detection of normal vibration modes of atomic force microscope cantilevers with the optical beam deflection method," *J. Appl. Phys.*, vol. 97, no. 8, p. 083524, 2005.
- [44] D. Kiracofe and A. Raman, "On eigenmodes, stiffness, and sensitivity of atomic force microscope cantilevers in air versus liquids," *J. Appl. Phys.*, vol. 107, no. 3, p. 033506, 2010.
- [45] K. S. Karvinen, M. G. Ruppert, K. Mahata, and S. O. R. Moheimani, "Direct tip-sample force estimation for high-speed dynamic mode atomic force microscopy," *IEEE Trans. Nanotechnol.*, vol. 13, no. 6, pp. 1257–1265, Nov. 2014.
- [46] D. Halim and S. O. R. Moheimani, "Reducing the effect of truncation error in spatial and pointwise models of resonant systems with damping," *Mech. Syst. Signal Process.*, vol. 18, no. 2, pp. 291–315, 2004.
- [47] I. R. Petersen and A. Lanzon, "Feedback control of negative-imaginary systems," *IEEE Control Syst.*, vol. 30, no. 5, pp. 54–72, Oct. 2010.
- [48] J. L. Fanson and T. K. Caughey, "Positive position feedback control for large space structures," *AIAA J.*, vol. 28, no. 4, pp. 717–724, 1990.
- [49] A. Lanzon and I. R. Petersen, "Stability robustness of a feedback interconnection of systems with negative imaginary frequency response," *IEEE Trans. Autom. Control*, vol. 53, no. 4, pp. 1042–1046, May 2008.
- [50] S. Patra and A. Lanzon, "Stability analysis of interconnected systems with 'mixed' negative-imaginary and small-gain properties," *IEEE Trans. Autom. Control*, vol. 56, no. 6, pp. 1395–1400, Jun. 2011.
- [51] S. Boyd and L. Vandenberghe, *Convex Optimization*. New York, NY, USA: Cambridge Univ. Press, 2004.
- [52] S. Boyd, L. El Ghaoui, E. Feron, and V. Balakrishnan, *Linear Matrix Inequalities in System and Control Theory*. Philadelphia, PA, USA: SIAM, 1994.
- [53] C. Scherer and S. Weiland, "Linear matrix inequalities in control," in *Lecture Notes*, vol. 1. Delft, The Netherlands: Dutch Institute of Systems and Control, 2000, pp. 1–241.
- [54] T. McKelvey, "Subspace methods for frequency domain data," in *Proc. Amer. Control Conf.*, vol. 1. Jun./Jul. 2004, pp. 673–678.
- [55] A. J. Fleming, "Dual-stage vertical feedback for high-speed scanning probe microscopy," *IEEE Trans. Control Syst. Technol.*, vol. 19, no. 1, pp. 156–165, Jan. 2011.
- [56] M. G. Ruppert and S. O. R. Moheimani, "A novel self-sensing technique for tapping-mode atomic force microscopy," *Rev. Sci. Instrum.*, vol. 84, no. 12, p. 125006, 2013.
- [57] M. G. Ruppert and S. O. R. Moheimani, "Novel reciprocal self-sensing techniques for tapping-mode atomic force microscopy," in *Proc. 19th IFAC World Congr.*, Cape Town, South Africa, Aug. 2014, pp. 7474–7479.
- [58] R. García and E. T. Herruzo, "The emergence of multifrequency force microscopy," *Nature Nanotechnol.*, vol. 7, pp. 217–226, Apr. 2012.



Michael G. Ruppert (S'14) received the Dipl.-Ing. degree in automation technology in production with a specialization in systems theory and automatic control from the University of Stuttgart, Stuttgart, Germany, in 2013. He is currently pursuing the Ph.D. degree in electrical engineering with The University of Newcastle, Callaghan, NSW, Australia.

He holds post-graduate research scholarships with The University of Newcastle and the Commonwealth Scientific and Industrial Research Organisation, Clayton, VIC, Australia. His current research interests include the utilization of system theoretic tools in multifrequency atomic force microscopy, multimode Q control of microcantilevers, and nanomechanical sensing.

Mr. Ruppert received the University of Stuttgart Academic Merit Scholarship and the Baden-Württemberg Scholarship.



S. O. Reza Moheimani (F'11) currently holds the James von Ehr Distinguished Chair in Science and Technology with the Department of Mechanical Engineering, University of Texas at Dallas, Richardson, TX, USA. His current research interests include ultrahigh-precision mechatronic systems, with a particular emphasis on dynamics and control at the nanometer scale, including applications of control and estimation in nanopositioning systems for high-speed scanning probe microscopy and nanomanufacturing, modeling and control of

microcantilever-based devices, control of microactuators in microelectromechanical systems, and design, modeling, and control of micromachined nanopositioners for on-chip scanning probe microscopy.

Dr. Moheimani is a fellow of the International Federation of Automatic Control and the Institute of Physics, U.K. His research has been recognized with a number of awards, including the IFAC Nathaniel B. Nichols Medal in 2014, the IFAC Mechatronic Systems Award in 2013, the IEEE Control Systems Technology Award in 2009, the IEEE TRANSACTIONS ON CONTROL SYSTEMS TECHNOLOGY Outstanding Paper Award in 2007, and several best paper awards in various conferences. He has served on the Editorial Boards of a number of journals, including the IEEE TRANSACTIONS ON MECHATRONICS, the IEEE TRANSACTIONS ON CONTROL SYSTEMS TECHNOLOGY, and *Control Engineering Practice*. He is currently the Chair of the IFAC Technical Committee on Mechatronic Systems, and has chaired several international conferences and workshops.